ARTICLE

Pillaring Chemically Exfoliated Graphene Oxide with Carbon Nanotubes for Photocatalytic Degradation of Dyes under Visible Light Irradiation

Li Li Zhang, Zhigang Xiong, and X. S. Zhao*

Department of Chemical and Biomolecular Engineering, National University of Singapore, 4 Engineering Drive 4, Singapore 117576

ABSTRACT Graphene oxide (GO) and reduced graphene oxide (RGO) platelets were pillared with carbon nanotubes (CNTs) by using the chemical vapor deposition (CVD) method with acetonitrile as the carbon source and nickel nanoparticles as the catalyst, aimed to prepare graphene-based materials with a high surface area and a good electrical conductivity. Characterization data showed that the composite materials with RGO layers pillared by CNTs formed a robust three-dimensional (3D) porous structure of specific surfaces as high as 352 m^2/g. The amount and length of the CNT pillars connecting the RGO layers were controlled by changing the amount of the nickel metal catalyst and the time of CVD. The CNT-pillared RGO composite materials exhibited an excellent visible light photocatalytic performance in degrading dye Rhodamine B because of the unique porous structure and the exceptional electron transfer property of graphene. Such CNT—RGO composites represent a new family of innovative carbon materials for visible-light-activated photocatalysis.

KEYWORDS: carbon nanotubes · graphene oxide · pillaring · photocatalysis · visible light

Graphene is rapidly gaining interest from a wide spectrum of research fields owing to its remarkable properties, such as high carrier mobility (200 000 $cm^2/(V \cdot s)$),[1] great mechanical strength,[2] and excellent thermal[3] and electrical conductivity.[4] The sp^2-hybridized carbon atoms within an ideal graphene sheet are highly efficient in storing and shuttling electrons.[5] Therefore, graphene or graphene-based materials hold a great promise in applications requiring fast electron transfer, such as field emission displays (FEDs),[6] energy storage,[7,8] and photocatalysis.[9]

We have observed an efficient electron transfer process between a photon-excited dye and reduced graphene oxide (RGO) under visible light irradiation.[9] The degradation of the dye was, however, observed to be kinetically slow because of the recombination of the injected electron and the excited dye. We have also found that deposition of gold (Au) nanoparticles can greatly accelerate the spatial separation of the injected electron and the excited dye, thus significantly improving the degradation of the dye under visible light irradiation *via* a mechanism different from that of traditional semiconductor photocatalysis.[9]

While a high theoretical specific surface area of graphene (2630 m^2/g) has been predicted,[10] experimentalists have yet succeeded in producing graphene with such a high surface area in spite of numerous research efforts.[11,12] A recent computation work of Froudakis and co-workers[7] predicted that a three-dimensional (3D) graphene nanostructure pillared by single-walled carbon nanotubes possesses a significantly enhanced hydrogen storage capacity. Inspired by this theoretical work, we attempted to pillar layered graphene oxide (GO) and RGO platelets with carbon nanotubes (CNTs) in the present work.

Scheme 1 illustrates the steps of preparing CNT-pillared GO and RGO 3D structures. First, chemically exfoliated GO or RGO platelets were dispersed in water in the presence of a surfactant. Then, a nickel nitrate solution was added under stirring at room temperature. Upon drying at 60 °C, Ni-containing GO or RGO platelets were obtained and subsequently used as the catalyst to grow CNTs using the chemical deposition (CVD) method with acetonitrile as the carbon source. Both the amount and the length of the CNTs were controlled by using amounts of Ni catalyst and CVD times. The final samples are denoted as GOCNT-*X*-*Y* or RGOCNT-*X*-*Y* for the CNT-pillared GO and RGO composites, respectively. Here, *X* represents CVD time (15 or 30 min) while *Y* refers to the Ni catalyst loading expressed using the mass ratio of Ni/C (here, Ni refers to the amount of nickel nitrate and C refers

*Address correspondence to chezxs@nus.edu.sg.

Received for review September 6, 2010 and accepted October 22, 2010.

Published online October 28, 2010. 10.1021/nn102308r

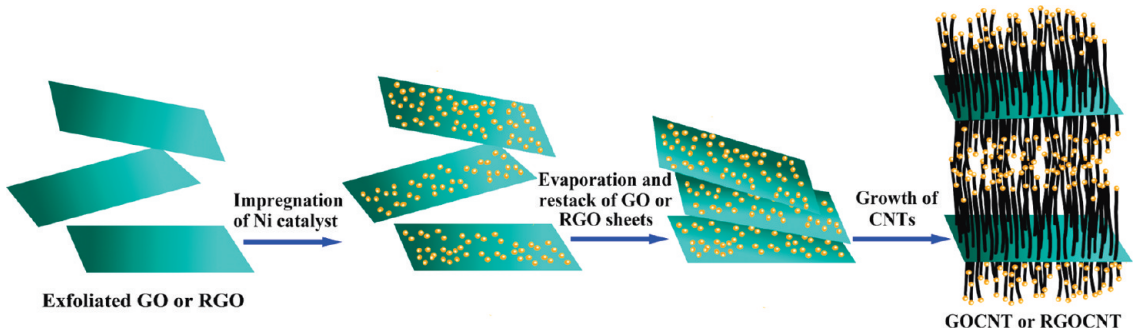

Scheme 1. Experimental steps of pillaring GO and RGO platelets with CNTs.

to the amount of GO or RGO used; see Supporting Information for details). For example, sample GOCNT-15-17 was prepared using Ni-containing GO with a Ni/GO ratio of 17 and the CVD time was 15 min, while sample RGOCNT-30-2 was obtained from Ni-containing RGO with a Ni/RGO ratio of 2 and the CVD time was 30 min.

Such 3D carbon structures are believed to display unique electronic and catalytic properties due to the synergetic effect between the RGO platelets and the CNT pillars. Indeed, the RGOCNT composite materials were found to exhibit an excellent performance in photocatalytic degradation of dye Rhodamine B (RhB) under visible light irradiation. To the best of our knowledge, this is the first experimental demonstration of pillaring chemically exfoliated GO with CNTs and exploration of such materials in photocatalytic degradation of dyes under visible light irradiation.

RESULTS AND DISCUSSION

Figure 1 shows the typical field emission scanning electron microscopy (FESEM) images of the GOCNT and RGOCNT samples. It can be seen that most of the CNTs grew perpendicularly to the normal of the GO and RGO platelets. The cross-section views of the samples clearly demonstrated a layered structure of the GO and RGO with CNTs as pillars between the GO and RGO platelets. It is also seen that increasing the amount of Ni catalyst led to the growth of more CNTs in the 3D nanostructure, while decreasing the CVD time resulted in a shorter length of the CNTs. The wall thickness and the inner diameter of the CNT were about 10 and 12 nm, respectively. The high-magnification transmission electron microscopy (TEM) image depicted in Figure 1h clearly shows the presence of straight graphene layers paralleling the axis of the CNTs. These ordered graphene layers with an interlayer distance of about 0.34 nm implied a high crystallinity of the CNTs, which are favorable for electron transport along the axis of the CNTs.[13]

The X-ray diffraction (XRD) patterns of the samples shown in Figure S1 (Supporting Information) confirmed the presence of pure metallic Ni (JCPDS No. 04-850), suggesting that it was the Ni metal nanoparticles that served as the catalytic sites for the growth of the CNTs within the GO and RGO platelets. The white dots seen from the FESEM images were Ni particles on the tips of the CNTs, implying that the growth of the CNTs followed the tip-growth model.[14] According to this model, the diameter of a CNT shall be comparable to the diameter of the metal catalyst on which it has grown. To confirm this, a sample (named GO-Ni) was prepared by treating a Ni-containing GO sample at 850 °C in the CVD reactor under nitrogen flow of 30 mL/min (similar to the experimental conditions of growing CNTs on the Ni-containing GO sample except for the absence of carbon precursor acetonitrile). The TEM image of sample GO-Ni shown in Figure S2 revealed that the sizes of the Ni particles were in the range of 30−40 nm, which are in good agreement with the diameters of the CNTs.

The Raman spectra of the CNT-pillared GO and RGO composites are shown in Figure 2. It can be seen that all samples exhibited the Raman peaks of the G band at about 1580 cm^{-1} and the D band at about 1348 cm^{-1}. The G band is a characteristic feature of graphitic carbon layers corresponding to the tangential vibration of the carbon atoms, whereas the D band is a typical sign of the presence of defective graphitic carbon.[15] The intensity ratio of the D and G peaks (I_D/I_G) gives a measure of the degree of crystallization and the alignment of the graphitic planes of the carbon materials.[15] The RGOCNT samples generally possessed a lower I_D/I_G value than the GOCNT samples, indicating a better crystallinity with less structural defects of the former. This result suggests that the RGOCNT composite has a better electrical conductivity than the GOCNT composite.

The solution-based electrochemical impedance spectroscopy (EIS) analysis data further supported the above conclusion. The EIS data were analyzed using the Nyquist plot method and are presented in Figure S3. The negligible high-frequency resistor-capacitor (RC) loops or semicircles for both of the GOCNT and the RGOCNT samples indicated a good electrode contact.[16] The 45° sloped portion of the Nyquist plots, the so-called Warburg resistance,[17] is a result of the frequency dependence of ion transport in the system. It can be seen that the RGOCNT sample possessed a smaller Warburg region, indicating a lower ion diffusion resistance and less obstruction of the ion movement, thus a better ion transport than the GOCNT sample.

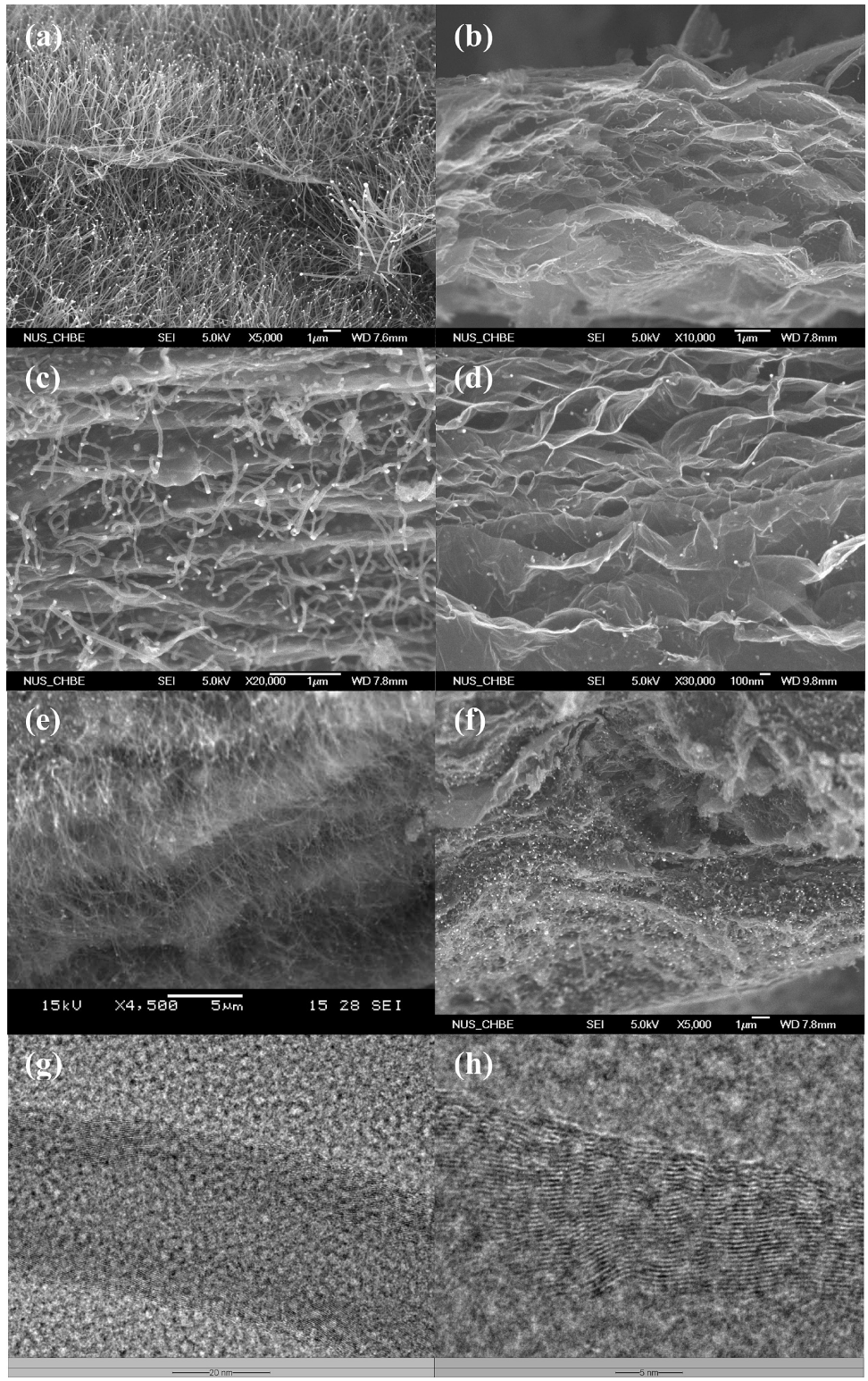

Figure 1. FESEM images of (a) GOCNT-30-17, (b) GOCNT-15-17, (c) GOCNT-30-9, (d) GOCNT-15-9, (e) RGOCNT-15-4, (f) RGOCNT-15-0.6 and TEM images of GOCNT-30-17 under different magnifications (g and h).

The composite materials were analyzed by using X-ray photoelectron spectroscopy (XPS), and the results are shown in Figure 3A. The two prominent peaks seen on the C1s XPS spectra of sample GO clearly indicated the presence of a considerable amount of oxygenated groups. After reduction (sample RGO), the C−O bond diminished while the C═C bond dominated, as evidenced by the presence of the peak at about 284.5 eV.[18] The GOCNT and RGOCNT samples displayed a C1s XPS spectrum similar to that of the RGO sample, suggesting that the CVD process resulted in a substantial loss in the oxygenated groups, especially for

the GOCNT composite. This observation is consistent with that reported in the literature.[19] The chemical composition of the samples according to the XPS results is summarized in Table 1. It can be seen that the oxygen contents for all composite samples were less than 8% (atomic concentration), which is very close to that of the pristine graphite. However, it should be noted that low oxygen content does not necessarily mean a better restoration of the $\pi-\pi$ conjugated plane in the final structure. Although thermal annealing removed some of the oxygen-containing groups from the GO sample, the process may not completely repair the holes and other defects may form within the carbon sheet.[20] Indeed, the Raman data showed the presence of a large amount of imperfections and defects on the GOCNT samples.

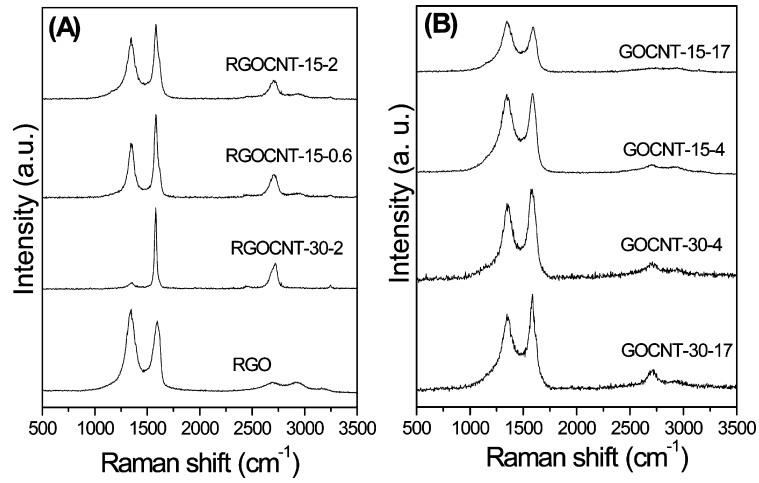

Figure 2. Raman spectra of (A) RGOCNT and (B) GOCNT samples.

The nitrogen adsorption−desorption isotherms of sample RGOCNT shown in Figure 3B (sample GOCNT exhibited a very similar isotherm to that of sample RGOCNT, thus is not presented here) displayed a type IV isotherm with a H2 hysteresis loop, indicating a mesoporous structure.[21,22] It can be seen from Table 1 that, upon pillaring with CNTs, the surface area was significantly increased. The most developed porosity was found from the samples pillared with shorter CNTs. The lower surface area and pore volume of the samples prepared with longer CVD times were probably due to the presence of dense CNTs in the samples.

The photocatalytic properties of the GOCNT and RGOCNT composites were evaluated using Rhodamine B (RhB) under visible light irradiation, and the results are shown in Figures 4. It is seen that RhB was very stable in the absence of a photocatalyst under visible light irradiation. It is also seen that no obvious degradation occurred in the dark, even with the presence of a photocatalyst. RhB was slightly degraded in the presence of catalyst GOCNT. However, the degradation of RhB was remarkably increased in the presence of the RGOCNT catalysts, especially those with a shorter length of CNTs. The photocatalytic reaction rates of the RGOCNT catalysts were faster than that of commercial photocatalyst P25. Table S1 (Supporting Information) summarizes the photocatalytic performance and some related physical properties of the photocatalysts. The highest photocatalytic degradation rate of RhB was calculated to be about 2.1×10^{-2} min^{-1} for sample RGOCNT-15-0.6, more than 4 times faster than that of P25 (4.9×10^{-3} min^{-1}). The UV−visible absorption intensity of RhB was gradually decreased with irradiation time (see Figure S4) without any shift of the absorption wavelength, suggesting a complete cleavage of RhB chromophores.[23] It is different from that carried out in a TiO_2 system, in which RhB was found to be gradually deethylated with a concomitant wavelength shift of its absorption band.[24]

The mechanism for the degradation of dyes under visible light irradiation over semiconductor (SC) photocatalysts, such as TiO_2, ZnO, and CeO_2,[25,26] is described as below: The dye is first excited by visible light, followed by electron transfer from the excited dye (dye*) to the conduction band of the SC. Then the electron is trapped by surface-adsorbed O_2 to generate various reactive oxygen species (ROSs).[24,27] The degradation efficiency greatly depends on the adsorption of the dye, the electron transfer between the dye* and the SC, and the electron recombination between $dye^{\bullet+}$ and SC^-.[27,28] On the other hand, the rate of the electron injection is determined by the redox potentials of the adsorbed dye* and the SC.

In the present work, the electron transfer from the excited dye (*e.g.*, RhB*) to graphene occurred under visible light irradiation, and the electron injection rate was much faster than that to TiO_2.[9] However, due to the fast recombination between the $RhB^{\bullet+}$ radicals and the injected electron, the degradation was significantly slowed. The Ni-containing CNTs are believed to be able to reduce the accumulation of the electron on graphene since the work functions of CNTs and Ni are, respectively, about −4.8 and −5.15 eV,[29,30] much

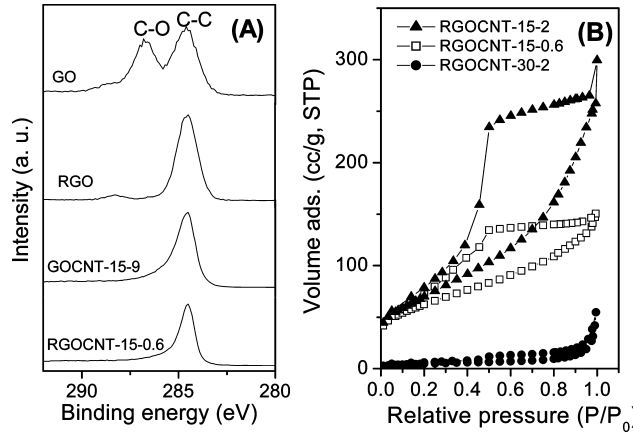

Figure 3. (A) C1s XPS spectra and (B) nitrogen adsorption−desorption isotherms of RGOCNT samples.

TABLE 1. Chemical Composition (atomic %) and Porosity of Samples

samples	C (%)	O (%)	C/O	S_{BET} (m^2/g)	V_{tot} (cm^3/g)	CVD time (min)
GOCNT-30-17	96.1	3.9	24.6	29	0.03	30
GOCNT-30-4	93.6	6.4	14.6	23	0.02	30
GOCNT-15-4	97.5	2.5	39.0	214	0.48	15
GOCNT-15-9	96.7	3.3	29.3	284	0.54	15
GOCNT-15-17	97	3	32.3	266	0.52	15
RGOCNT-30-2	94.1	5.9	15.9	26	0.04	30
RGOCNT-15-0.6	92.9	7.1	13.1	307	0.21	15
RGOCNT-15-2	91.5	8.5	10.8	352	0.38	15
RGOCNT-15-4	90.4	9.6	9.4	350	0.38	15

higher than that of graphene. Thus, in the presence of both CNTs and Ni, the injected electron on graphene plane can continuously transfer to the CNTs and Ni particles, spatially separating the $RhB^{\bullet+}$ radical and the electron, thus effectively decreasing electron accumulation, as schematically illustrated in Figure 5. Then the electron moved to the Ni particles was trapped by O_2 to produce various ROSs.

To prove the electron transfer between RhB and the RGOCNT catalysts, the fluorescence lifetimes of RhB were determined in different suspensions, and the results are shown in Table S1.[27] It can be seen that the RhB solution had a strong fluorescence with a lifetime of about 1.68 ns. Upon addition of TiO_2, RhB adsorbed on the surface of the TiO_2. The fluorescence lifetime of RhB thus decreased to 1.58 ns due to the electron transfer from RhB* to TiO_2.[27] When RGO was added to the RhB solution, the fluorescence lifetime decreased to 1.48 nm, indicating a faster electron transfer from RhB* to RGO than to TiO_2. For the CNT-pillared samples, the

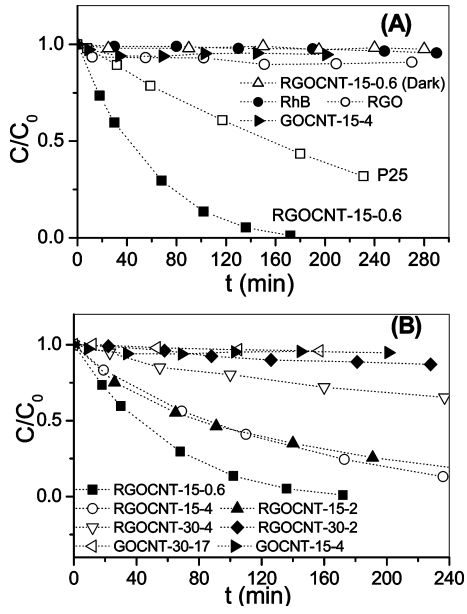

Figure 4. (A) Photocatalytic degradation for RhB under different experimental conditions with catalysts GOCNT-15-4 and P25. (B) Photocatalytic properties of different samples in degrading RhB.

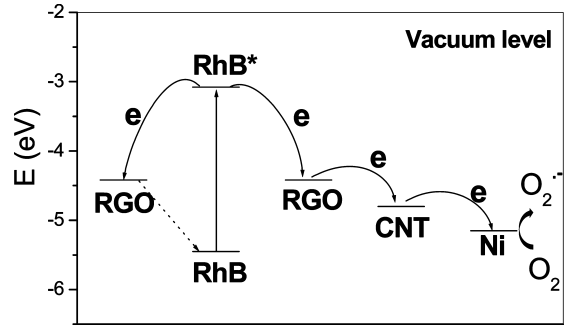

Figure 5. Energy diagram showing the proposed mechanism of photosensitized degradation of RhB under visible light irradiation.

electron could continuously move to the CNTs and Ni particles. Thus, the fluorescence lifetimes were further reduced to about 1.2 ns, indicating an enhanced electron transfer between RhB* and the RGOCNT catalysts.

On the basis of the above photosensitized degradation mechanism, the significantly different photoactivity between the GOCNT and RGOCNT catalysts can be attributed to the following two important factors. First, the adsorption of the dye on the GOCNT composites is much lower than that on the RGOCNT composites (see Table S1). Since the RGO platelets of the RGOCNT composite have a giant π-conjugational plane, it is very likely that RhB preferably adsorbed on the planar surface *via* a $\pi-\pi$ stacking with a face-to-face orientation.[31] However, such a π-conjugated plane was destroyed on the GO platelets of the GOCNT composite, leading to a poor interaction between the GOCNT catalyst and the dye. Second, the large amount of structural defects in the GO plane retarded the electron movement. Hence, no efficient electron transfer occurred between the excited dye and the GOCNT catalysts, as evidenced by the longer fluorescence lifetime of RhB*.

The length and amount of CNTs also greatly affected the photosensitized degradation of the dye. As is seen from Figure 4B, those RGOCNT photocatalysts with a shorter length of CNTs (RGOCNT-15-0.6, RGOCNT-15-2, and RGOCNT-15-0.6-4) were more reactive than P25, while those with a longer length of CNTs (RGOCNT-30-2 and RGOCNT-30-4) performed poorly as compared to P25. This can be explained by the different adsorption ability and the electron recombination probability. The RGOCNT catalysts with a shorter length of CNTs adsorbed more dye molecules than those with a longer length of CNTs (see Table S1). The higher specific surface area of the RGOCNT samples with a shorter length of CNTs (see Table 1) would be more advantageous toward dye adsorption. In addition, the growth of CNTs with a longer length on the RGO platelets inevitably led to a low surface of the composite so as to decrease the exposure of the $\pi-\pi$ conjugated plane in the RGO platelets. Besides the different dye adsorption abilities, the high probability of the electron recombina-

tion over the RGOCNT composite with longer CNT pillars may collectively account for the poorer photocatalytic performance. During the electron movement from the RGO surface to the long CNT chains, there is a high possibility that the electron was recombined with the $RhB^{\bullet+}$ adsorbed on the surface of the CNTs. The probability of such electron-radical recombination will be significantly reduced along short CNT chains. Moreover, since the Ni metal particle presented at the end of CNTs is a good electron mediator, surface-adsorbed O_2 could easily trap the electrons from the Ni particles to form various ROSs, leading to an efficient RhB degradation.

CONCLUSIONS

In summary, we have demonstrated the preparation of 3D CNT-pillared graphene oxide and reduced graphene oxide nanostructures with tunable length of the CNTs. Such nanostructures exhibited an excellent visible light photocatalytic performance in degrading RhB dye in water. The important findings in the present work include the following: (1) the growth of one-dimensional (1D) CNTs can be controlled by controlling the catalyst loading and the CVD time; (2) the use of the conducting carbon matrix such as reduced graphene oxide platelets is highly desirable for many applications requiring fast electron transfer such as catalysis (including photocatalysis), ion transportation, energy conversion, and storage; (3) the synergetic effect between the 1D CNTs and 2D reduced graphene oxide platelets effectively reduces the dynamic resistance of ion transport; and (4) the high adsorption ability toward organic dyes, strong $\pi-\pi$ interaction with dye chromophores, efficient photosensitized electron injection, and retarded electron-radical recombination enable the composite material to be an excellent photocatalyst for photoassisted degradation of dye pollutants in water.

METHODS

Preparation of GO and RGO. The GO dispersion was prepared by sonication of graphite oxide, which was obtained from natural graphite using a modified Hummers method.[32,33] Five grams of graphite and 2.5 g of $NaNO_3$ were mixed with 120 mL of H_2SO_4 (95 wt %) in a 500 mL flask. The mixture was stirred for 30 min within an ice bath. While maintaining vigorous stirring, 15 g of $KMnO_4$ was added. The rate of addition was carefully controlled to keep the reaction temperature below 20 °C. The ice bath was then removed, and the mixture was stirred at room temperature overnight. As the reaction progressed, the mixture gradually became pasty, and the color turned light brownish. At the end, 150 mL of deionized (DI) water was slowly added to the mixture under vigorous agitation. The reaction temperature was rapidly increased to 98 °C with effervescence, and the color changed to yellow. The diluted suspension was stirred for 1 day. Then, 50 mL of 30% H_2O_2 was added to the mixture. For purification, the mixture was washed by rinsing and centrifugation with 5% HCl and then DI water for several times to obtain the graphite oxide sample. The final GO dispersion was prepared by sonication of graphite oxide.

Reduction of GO was conducted by using the sodium borohydride reduction method: 0.3 g of GO was dispersed in 100 mL of DI water. The GO solution was sonicated for about 20 min; 0.4 g of sodium borohydride was then added, and the mixture was heated in an oil bath at 100 °C for 24 h. The final RGO sample was obtained after repeated washing with DI water followed by centrifugation.

Preparation of GOCNTs. A series of GOCNT samples containing different amounts and lengths of CNTs were prepared. In a typical preparation, 2 g of sodium dodecyl sulfate (SDS, Merck) was dissolved in 40 mL of DI water. Twenty milliliters of GO dispersion of concentration 5 mg/mL was added into the above solution. The mixture was sonicated for about 20 min. Then, 1.74 g of nickel nitrate hexahydrate ($Ni(NO_3)_2 \cdot 6H_2O$, Alfa Aesar) dissolved in 20 mL of DI water was added dropwise under vigorous stirring. The resulting mixture was diluted with DI water to have a total volume of 120 mL and heated to 90 °C under stirring. After 16 h, the mixture was evaporated and dried in air with a Petri dish at 60 °C for 24 h to obtain Ni-loaded GO platelets. To change the loading of Ni catalyst on the surface of GO, the Ni/C ratio, namely, the mass ratio of $Ni(NO_3)_2 \cdot 6H_2O$ over GO, was varied to be 4, 9, and 17. The amount of SDS was adjusted according to the amount of $Ni(NO_3)_2 \cdot 6H_2O$ added.

The growth of CNTs was conducted on the Ni-loaded GO platelets at 850 °C using the CVD method with acetonitrile as the carbon source as has been described previously.[34] The CVD deposition time was varied from 15 to 30 min to control the length of CNTs. The final solid products are denoted as GOCNT-*X*-*Y*, where *X* represents CVD time (15 or 30 min) while *Y* refers to the Ni catalyst loading expressed using Ni/C ratio. For example, sample GOCNT-15-17 was prepared using a Ni/GO ratio of 17 and a CVD time of 15 min, while GOCNT-30-17 was obtained from Ni/C ratio of 17 and CVD time of 30 min.

Preparation of RGOCNTs. The procedure for the preparation of RGOCNT nanocomposites was very similar to that of GOCNT, but with the addition of RGO dispersion rather than GO dispersion. The Ni/C ratio (mass ratio between $Ni(NO_3)_2 \cdot 6H_2O$ and RGO) was varied to be 0.6, 2, and 4. The growth of CNTs on the Ni-loaded RGO platelets followed exactly the same procedure as that described for GOCNT. The final products collected are denoted as RGOCNT-*X*-*Y*. For example, sample RGOCNT-15-2 was prepared by using a Ni/C ratio of 2 and a CVD time of 15 min and RGOCNT-30-2 was obtained from Ni/C ratio of 2 and CVD time of 30 min.

General Characterization. The microscopic feature of the samples was observed on a FESEM (JSM 6700F, JEOL Japan) operated at 10 kV and a TEM (JEM 2010, JEOL, Japan) operated at 200 kV. The pore structure of the sample was investigated using physical adsorption of nitrogen at the liquid-nitrogen temperature (77 K) on an automatic volumetric sorption analyzer (NOVA1100, Quantachrome). Prior to measurement, a sample was vacuum-degassed at 200 °C for 5 h. The specific surface area (S_{BET}) was determined according to the Brunauer−Emmett−Teller (BET) method in the relative pressure range of 0.01−0.2. The total pore volume (V_t) was obtained from the volume of nitrogen adsorbed at a relative pressure of 0.99. XRD patterns were collected on an XRD-6000 (Shimadzu, Kyoto, Japan) with Cu Kα radiation ($\lambda = 1.5418$ Å) as the X-ray source. XPS analysis was carried out on an AXIS HSI 165 spectrometer (Kratos Analytical) using a monochromatized Al Kα X-ray source (1486.71 eV). The Raman spectra were carried out using a WITEC CRM200 Raman system with a 532 nm laser (2.33 eV) source and 100× objective lens. The EIS was collected using an Autolab PGSTAT302N at room temperature.

Measurement of Photoactivity Properties. Photocatalytic degradations were carried out in an open thermostatic photoreactor. Before irradiation, a suspension containing 100 mL of 5.3×10^{-3} mM RhB solution and 6.0 mg of solid catalyst was sonicated for 5 min and stirred for 30 min in the dark to allow sorption equilibrium. Then, the mixture was irradiated with a 350 W xenon lamp equipped with a 420 nm cutoff filter. At a given time inter-

val of irradiation, 5 mL aliquots were withdrawn. The residual concentration of RhB in the aliquots was analyzed using a Shimadzu 1601 PC UV−vis spectrophotometer.

Acknowledgment. Financial support from Ministry of Education of Singapore (Project MOE2008-T2-1-004) and from Environment and Water Industry Development Council (EWI) of Singapore (Project MEWR 651/06/161) is greatly appreciated.

Supporting Information Available: XRD patterns, TEM images, EIS analysis data, and photocatalytic properties of samples. This material is available free of charge *via* the Internet at http://pubs.acs.org.

REFERENCES AND NOTES

1. Bolotin, K. I.; Sikes, K. J.; Jiang, Z.; Klima, M.; Fudenberg, G.; Hone, J.; Kim, P.; Stormer, H. L. Ultrahigh Electron Mobility in Suspended Graphene. *Solid State Commun.* **2008**, *146*, 351–355.
2. Lee, C.; Wei, X.; Kysar, J. W.; Hone, J. Measurement of the Elastic Properties and Intrinsic Strength of Monolayer Graphene. *Science* **2008**, *321*, 385–388.
3. Balandin, A. A.; Ghosh, S.; Bao, W.; Calizo, I.; Teweldebrhan, D.; Miao, F.; Lau, C. N. Superior Thermal Conductivity of Single-Layer Graphene. *Nano Lett.* **2008**, *8*, 902–907.
4. Park, S.; Ruoff, R. S. Chemical Methods for the Production of Graphenes. *Nat. Nanotechnol.* **2009**, *4*, 217–224.
5. Stankovich, S.; Dikin, D. A.; Dommett, G. H. B.; Kohlhaas, K. M.; Zimney, E. J.; Stach, E. A.; Piner, R. D.; Nguyen, S. T.; Ruoff, R. S. Graphene-Based Composite Materials. *Nature* **2006**, *442*, 282–286.
6. Yoon, H.; Seo, K.; Bagkar, N.; In, J.; Park, J.; Kim, J.; Kim, B. Vertical Epitaxial Co_5Ge_7 Nanowire and Nanobelt Arrays on a Thin Graphitic Layer for Flexible Field Emission Displays. *Adv. Mater.* **2009**, *21*, 4979–4982.
7. Dimitrakakis, G. K.; Tylianakis, E.; Froudakis, G. E. Pillared Graphene: A New 3-D Network Nanostructure for Enhanced Hydrogen Storage. *Nano Lett.* **2008**, *8*, 3166–3170.
8. Zhang, L. L.; Zhou, R.; Zhao, X. S. Graphene-Based Materials as Supercapacitor Electrodes. *J. Mater. Chem.* **2010**, *20*, 5983–5992.
9. Xiong, Z.; Zhang, L. L.; Ma, J.; Zhao, X. S. Photocatalytic Degradation of Dyes over Graphene−Gold Nanocomposites under Visible Light Irradiation. *Chem. Commun.* **2010**, *46*, 6099–6101.
10. Stoller, M. D.; Park, S.; Yanwu, Z.; An, J.; Ruoff, R. S. Graphene-Based Ultracapacitors. *Nano Lett.* **2008**, *8*, 3498–3502.
11. Lv, W.; Tang, D.-M.; He, Y.-B.; You, C.-H.; Shi, Z.-Q.; Chen, X.-C.; Chen, C.-M.; Hou, P.-X.; Liu, C.; Yang, Q.-H. Low-Temperature Exfoliated Graphenes: Vacuum-Promoted Exfoliation and Electrochemical Energy Storage. *ACS Nano* **2009**, *3*, 3730–3736.
12. Wang, Y.; Shi, Z.; Huang, Y.; Ma, Y.; Wang, C.; Chen, M.; Chen, Y. Supercapacitor Devices Based on Graphene Materials. *J. Phys. Chem. C* **2009**, *113*, 13103–13107.
13. Javey, A.; Guo, J.; Wang, Q.; Lundstrom, M.; Dai, H. Ballistic Carbon Nanotube Field-Effect Transistors. *Nature* **2003**, *424*, 654–657.
14. Otsuka, K.; Abe, Y.; Kanai, N.; Kobayashi, Y.; Takenaka, S.; Tanabe, E. Synthesis of Carbon Nanotubes on Ni/Carbon-Fiber Catalysts under Mild Conditions. *Carbon* **2004**, *42*, 727–736.
15. Tuinstra, F.; Koenig, J. L. Raman Spectrum of Graphite. *J. Chem. Phys.* **1970**, *53*, 1126–1130.
16. Portet, C.; Lillo-Rodenas, M. A.; Linares-Solano, A.; Gogotsi, Y. Capacitance of KOH Activated Carbide-Derived Carbons. *Phys. Chem. Chem. Phys.* **2009**, *11*, 4943–4945.
17. Kotz, R.; Carlen, M. Principles and Applications of Electrochemical Capacitors. *Electrochim. Acta* **2000**, *45*, 2483–2498.
18. Gao, W.; Alemany, L. B.; Ci, L.; Ajayan, P. M. New Insights into the Structure and Reduction of Graphite Oxide. *Nat. Chem.* **2009**, *1*, 403–408.
19. Yang, D.; Velamakanni, A.; Bozoklu, G.; Park, S.; Stoller, M.; Piner, R. D.; Stankovich, S.; Jung, I.; Field, D. A.; Ventrice, C. A., Jr. Chemical Analysis of Graphene Oxide Films after Heat and Chemical Treatments by X-ray Photoelectron and Micro-Raman Spectroscopy. *Carbon* **2009**, *47*, 145–152.
20. Li, X.; Zhang, G.; Bai, X.; Sun, X.; Wang, X.; Wang, E.; Dai, H. Highly Conducting Graphene Sheets and Langmuir−Blodgett Films. *Nat. Nanotechnol.* **2008**, *3*, 538–542.
21. Kruk, M.; Jaroniec, M. Gas Adsorption Characterization of Ordered Organic−Inorganic Nanocomposite Materials. *Chem. Mater.* **2001**, *13*, 3169–3183.
22. Gregg, S. J.; Sing, K. S. W. *Adsorption, Surface Area and Porosity*, 2nd ed.; Academic Press, Inc.: New York, 1982.
23. Liu, G. M; Li, X. Z; Zhao, J. C; Hidaka, H; Serpone, N. Photooxidation Pathway of Sulforhodamine-B. Dependence on the Adsorption Mode on TiO_2 Exposed to Visible Light Radiation. *Environ. Sci. Technol.* **2000**, *34*, 3982–3990.
24. Wu, T.; Liu, G.; Zhao, J.; Hidaka, H.; Serpone, N. Photoassisted Degradation of Dye Pollutants. V. Self-Photosensitized Oxidative Transformation of Rhodamine B under Visible Light Irradiation in Aqueous TiO_2 Dispersions. *J. Phys. Chem. B* **1998**, *102*, 5845–5851.
25. Ji, P. F.; Zhang, J. L.; Chen, F.; Anpo, M. Study of Adsorption and Degradation of Acid Orange 7 on the Surface of CeO_2 under Visible Light Irradiation. *Appl. Catal., B* **2009**, *85*, 148–154.
26. Li, Y. Z.; Xie, W.; Hu, X. L.; Shen, G. F.; Zhou, X.; Xiang, Y.; Zhao, X. J.; Fang, P. F. Comparison of Dye Photodegradation and Its Coupling with Light-to-Electricity Conversion over TiO_2 and ZnO. *Langmuir* **2010**, *26*, 591–597.
27. Kamat, P. V. Photochemistry on Nonreactive and Reactive (Semiconductor) Surfaces. *Chem. Rev.* **1993**, *93*, 267–300.
28. Zhao, D.; Chen, C.; Wang, Y.; Ma, W.; Zhao, J.; Rajh, T.; Zang, L. Enhanced Photocatalytic Degradation of Dye Pollutants under Visible Irradiation on Al(III)-Modified TiO_2: Structure, Interaction, and Interfacial Electron Transfer. *Environ. Sci. Technol.* **2008**, *42*, 308–314.
29. Yao, Y.; Li, G.; Ciston, S.; Lueptow, R. M.; Gray, K. A. Photoreactive TiO_2/Carbon Nanotube Composites: Synthesis and Reactivity. *Environ. Sci. Technol.* **2008**, *42*, 4952–4957.
30. Godard, G.; de Mallmann, A.; Candy, J. P.; Fiddy, S.; Basset, J. M. Reductive Adsorption of Cd^{2+} on a Nickel Surface in Aqueous Solution: Characterization of Surface Adatoms by *In Situ* EXAFS. *J. Phys. Chem. C* **2008**, *112*, 12936–12942.
31. Zhang, H.; Lv, X.; Li, Y.; Wang, Y.; Li, J. P25-Graphene Composite as a High Performance Photocatalyst. *ACS Nano* **2009**, *4*, 380–386.
32. Hummers, W. S.; Offeman, R. E. Preparation of Graphitic Oxide. *J. Am. Chem. Soc.* **1958**, *80*, 1339.
33. Zhang, K.; Zhang, L. L.; Zhao, X. S.; Wu, J. Graphene/Polyaniline Nanofiber Composites as Supercapacitor Electrodes. *Chem. Mater.* **2010**, *22*, 1392–1401.
34. Su, F.; Zhao, X. S.; Wang, Y.; Lee, J. Y. Bridging Mesoporous Carbon Particles with Carbon Nanotubes. *Microporous Mesoporous Mater.* **2007**, *98*, 323–329.